Prediction of Time-Mean Atmospheric Circulation and Rainfall: Influence of Pacific Sea Surface Temperature Anomaly

J. SHUKLA AND M. J. FENNESSY

Center for Ocean–Land–Atmosphere Interactions, Department of Meteorology, University of Maryland, College Park, Maryland

(Manuscript received 21 January 1987, in final form 27 May 1987)

ABSTRACT

A global general circulation model was integrated for 60 days with the observed initial conditions at 0000 UTC on 15, 16 and 17 December 1982 and climatological boundary conditions of sea surface temperature (SST), soil moisture, snow cover, sea ice and albedo. These integrations were repeated after the observed SST anomalies over the Pacific Ocean during the winter of 1982–83 were added to the climatological SST. Model forecasts for 10-, 30- and 60-day averages of circulation and rainfall were examined.

A comparison of the model-predicted, time-averaged circulation and rainfall anomaly with the corresponding observations show that the inclusion of the sea surface temperature (SST) anomalies over the Pacific Ocean produces spectacular improvements in the forecasts of tropical circulation and rainfall. There is also clear improvement in the forecasts of extratropical circulation, especially after the model drift is removed from the forecasts. The model drift was calculated as the mean difference between the model forecasts with climatological boundary conditions for the five different and independent initial conditions (at 0000 UTC on 1 January 1979, 1980, 1981, 1982 and 1984) and the corresponding verifying observations. Due to an insufficient number of forecasts for defining the model drift, only a zonally symmetric model drift was removed from the forecasts. This study, like several other similar studies, clearly demonstrates that if SST anomalies could be predicted in advance, it would be possible to make substantial improvements in long range prediction over the tropics and also, to a limited extent, over the midlatitudes.

1. Introduction

A possible conceptual framework to examine the questions related to the variability and predictability of monthly and seasonal average atmospheric circulations is to consider separately the roles of the internal dynamical processes and the changes in the boundary conditions at the earth's surface (Charney and Shukla, 1981). Such a framework makes it convenient to interpret the results of a large number of observational and modeling studies which are designed to investigate the influence of a particular boundary forcing. In an earlier paper it was suggested that in the classical predictability sense the monthly average circulations should be predictable using complex general circulation models (GCMs) of the atmosphere (Shukla, 1981). This conclusion was based on the following model-derived results: (a) planetary-scale waves are more predictable than the synoptic-scale waves; (b) it is the predictability of the low-frequency planetary scale waves that is important for the prediction of monthly averages; and (c) the combined effects of the unpredictability of the planetary scale waves and the degradation of their predictability due to interactions with the unpredictable synoptic scale waves is not large enough to make the monthly averages unpredictable. In other words, the limit of deterministic prediction of about 2 weeks based on classical predictability studies does not apply to the predictability of space–time averages, because the former refers to the predictability of instantaneous flows described by locations and intensities of the individual synoptic scale disturbances, whereas, the latter refers to the average properties of the flow for which the errors in prediction of individual disturbances is considerably reduced. These conclusions did not necessarily mean that useful monthly forecasts can actually be made with GCMs, particularly because the GCMs have a tendency to drift to their own climate rather quickly, and the errors simply due to the climate drift could be large enough within a month to make the monthly forecasts useless. It was conjectured, however, that if the interactions between the climate drift and the transient evolution of the initial flow were not too strong, and if the errors due to climate drift were quasi-systematic, they could be removed from the model-produced forecasts (Shukla, 1983). A recent pioneering study by Miyakoda, et al. (1986) lends further support both to the concept of the dynamical predictability of monthly means and to the conjecture of the weak interaction between the climate drift and the transient evolution of the initial flow. Their results provide convincing evidence that

Corresponding author address: Dr. Jagadish Shukla, Center for Ocean-Land-Atmosphere, Interactions, University of Maryland, College Park, MD 20742.

the dynamical structure of the initial flow, and particularly of its planetary wave component, has sufficient memory of its own that a realistic nonlinear dynamical model can produce useful forecasts of 30-day averages.

In the papers referred to the possible role of the boundary conditions in enhancing the predictability of monthly and seasonal averages was also considered, but not investigated. Based on a review of several observational and modeling studies, it was suggested that the inclusion of the effects of the boundary conditions at the earth's surface has the potential to further enhance the predictability of monthly and seasonal averages (Shukla, 1984).

The present research is one such attempt to investigate the impact of using correct SST boundary conditions in the Pacific Ocean on prediction of 30- and 60-day average circulation and rainfall. The improvements in the prediction of the time averaged circulation due to the correct specification of SST anomalies in the equatorial Pacific, alone, are found to be large enough to validate the suggestion that a correct treatment of the boundary conditions of global SST, soil moisture, sea ice and snow, etc., could further enhance the prediction of the space–time average circulation of the atmosphere. It should be noted, however, that the observed SST anomaly during 1982–83 was one of the largest ever observed, and more prediction experiments need to be carried out to determine the quantitative effects of other boundary conditions observed during other years.

Mechanisms through which changes in the different boundary conditions influence the changes in the atmospheric circulation have been previously summarized in various papers (Namias, 1978; Shukla, 1984; Walsh et al. 1985) and it is sufficient to state that the physical processes which give rise to anomalous atmospheric circulation due to anomalous boundary forcing are different for different types of boundary forcings over land and ocean. These influences depend not only on the magnitude and the spatial scale of the boundary anomaly, but also on the structure of the dynamical flow which interacts with the lower boundary, and therefore it is not possible to infer the possible influences in advance. It is necessary to perform a numerical integration of a GCM to determine the influence of the boundary condition as it depends upon the structure of the initial large-scale flow whose evolution we wish to predict. In this study we have started integration from the observed initial conditions during December 1982 and made 60-day predictions with and without the observed SST anomalies in the Pacific Ocean, while examining their impact on prediction.

2. Influence of equatorial Pacific SST anomalies on atmospheric circulation

Recently several scientific papers have appeared in which the influence of tropical SST anomalies on atmospheric circulation has been investigated by carrying out controlled numerical experiments with dynamical models of varying degrees of complexity. In order to better define the context in which the present study has been carried out, and also, in order to provide a suitable interpretation of the present results, we have summarized below the conclusions and our interpretations of earlier investigations.

Results of GCM sensitivity to equatorial Pacific SST anomalies have been reported by Rowntree (1972), Julian and Chervin (1978), Rowntree (1979), Keshavamurty (1982), Blackmon et al. (1983), Shukla and Wallace (1983), Palmer and Mansfield (1984), Fennessy et al. (1985), Geisler et al. (1985), Tokioka et al. (1985), Boer (1985), Cubash (1985), Michaud et al. (1985), Suarez (1985), and Palmer and Mansfield (1986a, 1986b). Based on the results of such numerical experiments and other more theoretical investigations (viz., Webster, 1981; Hoskins and Karoly, 1981) a conceptual model for the mechanisms through which SST anomalies influence the model atmosphere has been described by Shukla (1986). The basic concepts and the key results of the numerical experiments can be summarized as follows:

(i) SST anomalies, particularly in the tropics, can produce significant changes in the atmospheric circulation, locally and remotely, only if the magnitude and the spatial scale of the anomaly, and the structure of the mean SST field and the large scale dynamical circulation are such that the surface sensible and latent heat flux anomalies can be transformed into a deeper heating anomaly in the atmosphere.

(ii) Warm SST anomalies over relatively warmer mean background SST in areas of large-scale, low-level convergence in the tropics are more favorable for producing deep heating anomalies than the regions of colder mean background SST and large-scale low-level divergence.

(iii) The tropical response strongly depends upon the shape and size of the SST anomaly and its location with respect to the large scale SST field; its dependence upon the initial conditions of the atmospheric flow fields is rather weak. On the other hand, the midlatitude response to the tropical SST anomalies (and therefore tropical heating fields) strongly depends upon the structure and variability of the large-scale dynamical circulation. Therefore, two different GCMs with different climatologies of stationary and transient variability can produce quite different midlatitude responses for the same tropical SST anomaly.

(iv) The time it takes for a GCM simulation to be influenced by a prescribed SST anomaly depends upon the time it takes for the surface anomaly to be transformed into a deep heat source which, in turn, depends upon the physical parameterizations of the model. It is therefore likely that if the boundary layer and convection parameterizations in a GCM are such that it

takes too long to transmit the boundary anomaly to the interior, the GCM would not show any influence of the changes in the boundary conditions on medium-range prediction.

(v) The midlatitude equilibrium (long term mean) response of a tropical SST anomaly depends upon the mean climate of the model, but the transient response (especially the first 30 days) depends mainly upon the structure of the initial conditions of the atmospheric flow.

The general approach of earlier GCM studies has been to conduct sensitivity experiments in which the model's numerical response to the prescribed SST anomalies has been investigated by integrating the model with and without the SST anomalies and examining the difference between the two model integrations as a possible response to the prescribed SST anomaly.

This study differs in one important respect: we would like to investigate the impact of SST anomalies on the skill of the 30–60 day prediction. We start our integrations with observed initial conditions and we verify our results against the actual atmospheric observations. The present study is a natural extension of the past investigations; the cumulative results have given us enough confidence to initiate actual prediction experiments. In order to make our results comparable with the earlier investigations, we have also examined the results as classical sensitivity experiments by presenting differences in GCM simulations with and without the SST anomaly.

In section 3 we have described the results of several model integrations with climatological boundary conditions. These integrations were required in order to determine the systematic forecast errors which will be referred to as the model drift. In section 4 we will describe the initial conditions, the boundary conditions and the experimental design. In section 5, we present the results of the integrations and forecast verification, and in section 6, we present a summary and concluding remarks.

3. The model, the model climatology and the model drift

The GLAS climate model used for this study is global in extent with a 4° latitude by 5° longitude grid and nine sigma levels in the vertical. The PBL in the model is that of Deardorff (1972) as modified by Randall (1976). Supersaturation clouds occur at all nine levels, while convective clouds (Arakawa, 1969) are limited to the lowest six levels. Only the lowest six levels of supersaturation clouds interact with radiation. The Matsuno scheme is used for time integration with a 7½ min time step. Shortwave radiation and other physical processes are calculated each simulated half-hour, with the exception of longwave radiation which is calculated at 5-h intervals and applied at each half-hour. This model and the climatological boundary conditions used are identical to those used and described by Fennessy et al. (1985).

In order to analyze the model climatology and determine the model climate drift, five 60-day integrations were carried out using seasonally varying climatological boundary conditions of SST, soil moisture, sea ice and snow cover. These integrations were started from NMC analyses of 0000 UTC on 1 January 1979, 1980, 1981, 1982 and 1984. All future references to the model climatology will be referring to the average of these five integrations. The observed analyses at 12-h intervals for the same five 60-day periods were also obtained from NMC. All future references to the observed climatology will be referring to the average of these five analyses. Five years of observations would normally be considered too few to obtain a reliable climatology. However, our aim here is not to use the "best" available observed climatology, but to use the observed climatology most appropriate to compare with our model climatology. The difference (model climatology minus observed climatology) gives the model climate drift. It would have been desirable to have many more integrations to determine the model drift; however, the zonally averaged character of the drift is so repetitive in each of the five integrations that we feel justified in calculating the zonally averaged drift from five cases only. It is only the zonally averaged climate drift that is removed from the model forecasts before verification against the actual observations.

The 1–5 day average drift in the zonally averaged temperature field (Fig. 1a) already displays a negative bias at upper levels in the polar regions. By days 11–15 (Fig. 1b), this negative bias has increased to over 5 deg in the upper levels, while expanding throughout most of the troposphere. By days 56–60, the last 5 day average in the climatology, this negative drift has reached over 20 deg in the polar regions at the upper levels and is 3 deg or more almost everywhere, with the exception of the tropics (Fig. 1c). The 1–60-day average drift (Fig. 1d) resembles the 56–60-day drift except it has about one-half the magnitude, suggesting a quasi-linear growth of the extratropical model drift.

The observed 60-day climatology of the zonally averaged zonal wind contains subtropical jets with maxima between 200 and 300 mb (Fig. 2a). The model climatological zonal wind profile correctly simulates the position and magnitude of the subtropical jets up to about 200 mb (Fig. 2b). Above 200 mb the model jets are too strong, particularly the winter jet which continues to increase with height. The model correctly simulates the tropical easterlies below 500 mb, although at upper levels, unlike the observed, the simulated tropical zonal wind is westerly.

The model's 60-day climatology of sea level pressure (SLP) is quite reasonable with respect to the observed climatology (not shown). The major discrepancy is that compared to observations, the model SLP is higher

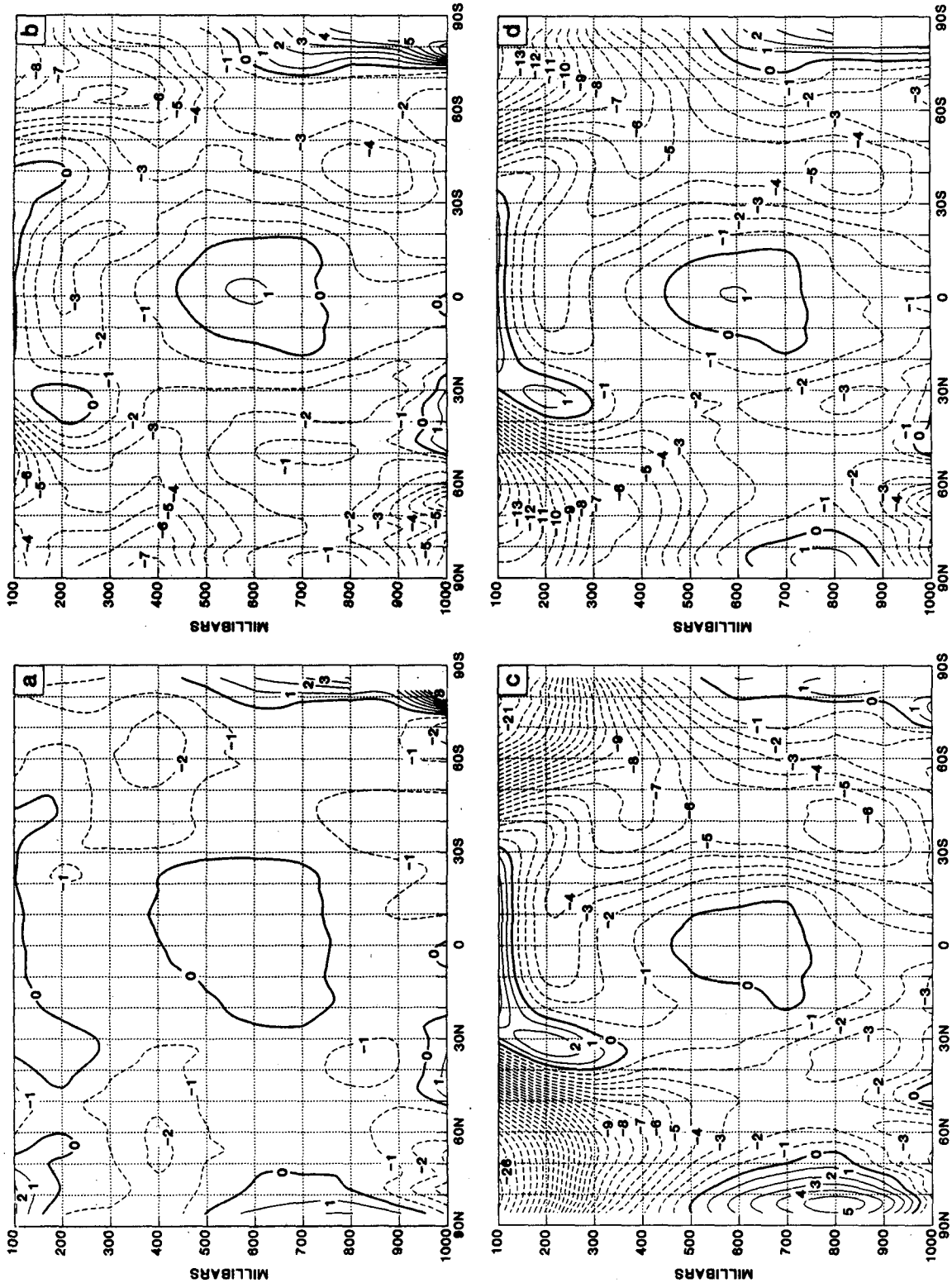

FIG. 1. Zonally averaged time mean model drift for temperature (°C) (model 5-yr climatology—observed 5-yr climatology) for (a) 1–5 day, (b) 11–15 day, (c) 56–60 day, and (d) 1–60 day. Dashed contours are negative.

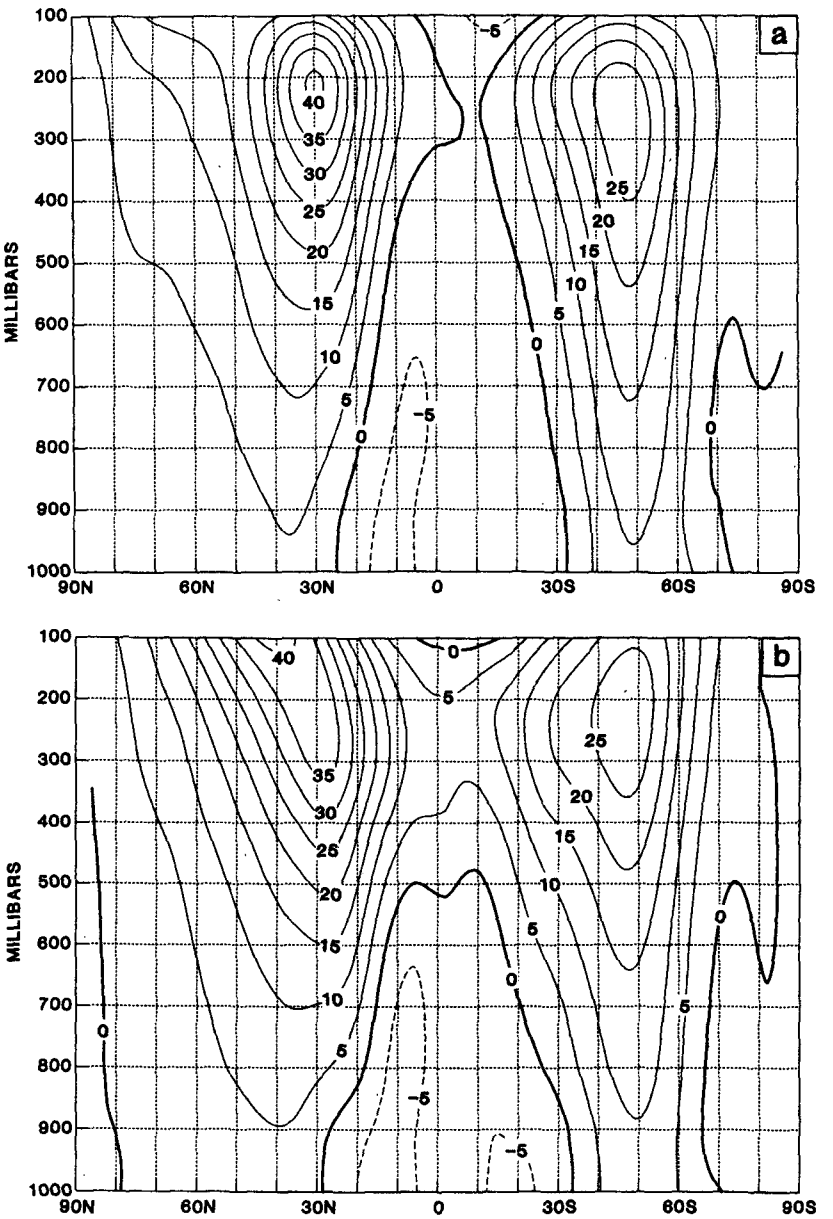

FIG. 2. Time mean (1–60 day) zonally averaged zonal wind (m s^{-1}) for (a) 5-yr observed climatology and (b) 5-yr model climatology. Dashed contours are negative.

over the oceans and lower over the continents in the Northern Hemisphere.

The 60-day 300-mb geopotential drift (Fig. 3) is dominantly negative, reflecting the cold bias seen in the zonal temperature drift field (Fig. 1d). It is rather interesting to note that the drift in the geopotential height field in the northern hemisphere is very similar to that in one version of the GFDL Model (Miyakoda et al. (1986, Fig. 6).

The observed December, January, February (DJF) climatological precipitation (Fig. 4a) was calculated from a 7 year outgoing longwave radiation (OLR) climatology using an empirical formula (Arkin, personal communication). The empirical formula is

$$\text{precipitation (mm/day)} = (25.4/30) \times (63.9 - 0.22\ \text{OLR})$$

where OLR represents the outgoing longwave radiation in W m^{-2}. The areas of heavy rainfall in the model 60-day climatological precipitation (Fig. 4b) compare well with the observations. The observed rainfall maxima over Indonesia and South America are simulated reasonably well; however, the model tends to produce

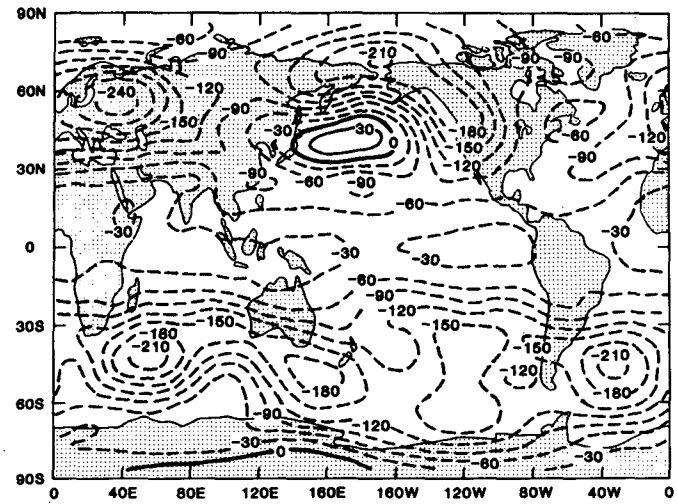

FIG. 3. Time mean (1–60 day) model drift for 300-mb geopotential height (meters) (model 5-yr climatology—observed 5-yr climatology). Dashed contours are negative.

precipitation across the whole equatorial region rather than placing it in the South Pacific convergence zone (SPCZ), as observed.

We do not have any satisfactory explanation for the fine structures in the maps of climate drift (see for example, Fig. 3). Although we believe that a large part of the zonal asymmetry of the model drift is genuine, we are not confident that five cases are enough to define the three-dimensional character of the climate drift because the influence of the individual initial conditions could be quite large. We have, therefore, chosen only to remove the zonally averaged climate drift from the forecasts described in the later sections. It is possible that the improvements in the model forecasts would be even larger if the three-dimensional climate drift could be reliably calculated and removed from the model forecasts.

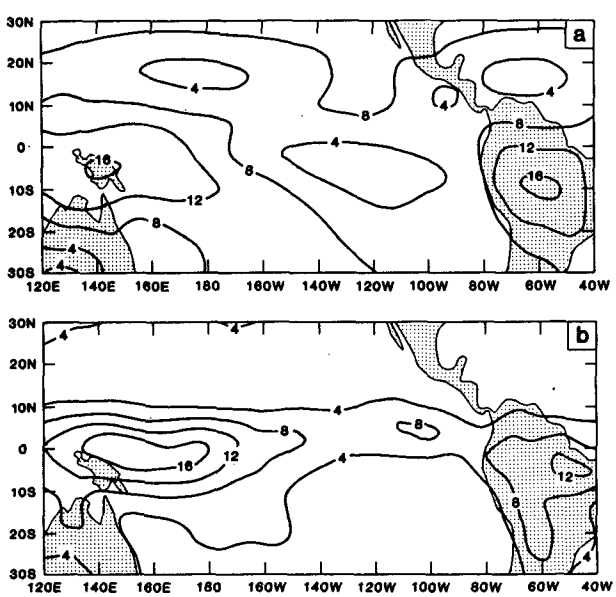

FIG. 4. (a) The DJF mean observed climatology of precipitation (mm day^{-1}) calculated from 7-yr OLR climatology. (b) 1–60 day average 5-yr model climatology of precipitation. Contour interval is 4 mm day^{-1}.

4. Initial and boundary conditions

Three observed initial conditions (ICs) from the NMC analyses for 0000 UTC on 15, 16 and 17 December, 1982 were used. For each initial condition, two model integrations were carried out until 15 February 1983 using climatological boundary conditions (to be referred to as control (C) integrations) and observed SST over the Pacific Ocean during 1982–83 (to be referred to as boundary change (B) integrations). The initial condition for the 300-mb geopotential height on 16 December is shown in Fig. 5a. The difference in the 300-mb geopotential height between the average of the three ICs and the 5-yr observed January climatology is shown in Fig. 5b. Notable are the deep Aleutian and Icelandic lows and the ridging over North America and Eurasia relative to the January Climatology. To illustrate how different the initial conditions are from each other, the difference in the 300-mb geopotential height between 15 December and 17 December is shown in Fig. 5c. At some grid points this difference exceeds 500 m.

The climatological SST for January used in the control simulations is shown in Fig. 6a. The corresponding SST used in the boundary simulations is shown in Fig. 6b. The SST for the boundary forecasts was obtained by adding the observed monthly SST anomalies for December 1982, January 1983 (Fig. 6c) and February

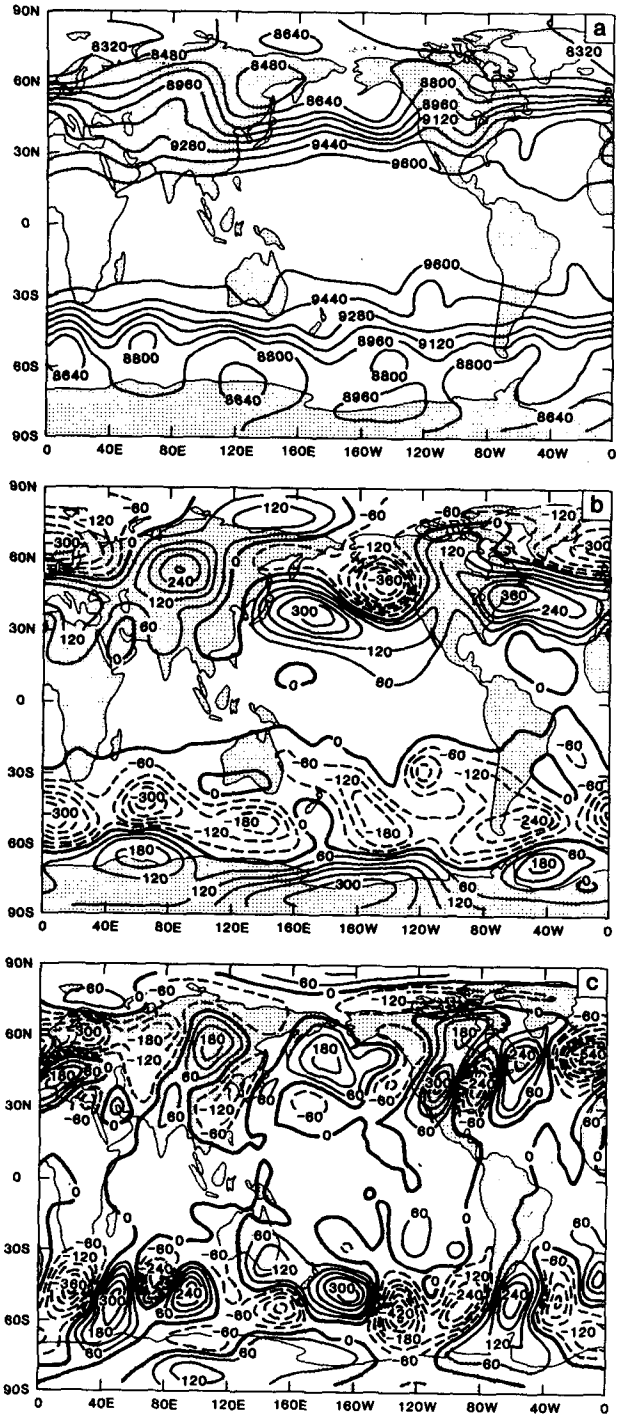

FIG. 5. Geopotential height (meters) at 300 mb for (a) 16 December 1982 initial condition; (b) average of three initial conditions (15, 16 and 17 December 1982) minus 5-yr January observed climatology; and (c) 17 December 1982 initial condition minus 15 December 1982 initial condition. Dashed contours are negative.

1983 to the respective monthly climatological SST for the region of the Pacific from 40°S to 60°N. The SST anomaly was obtained from the Climate Analysis Center. During the integration, the SST at the model grid points is updated daily by linear interpolation from the monthly SST.

5. Results

The results are presented in three sections. Subsection 4a describes the time mean observed and forecast anomaly fields. In subsection 4b the time evolution of some features of the anomalous circulation are presented. Finally, in subsection 4c the forecasts are evaluated in terms of root-mean-square (rms) error and anomaly correlation coefficient (ACC).

a. Time mean anomalies

Two types of time mean model-simulated anomalies are compared with the time-mean observed anomalies. The first type of simulated anomaly is calculated by subtracting the average of the three control integrations from the average of the three boundary integrations. This method of calculating the anomalies emphasizes the effects of the anomalous boundary conditions only, because contributions from the initial conditions are removed which can be significant either due to persistence or due to the evolution of circulation features

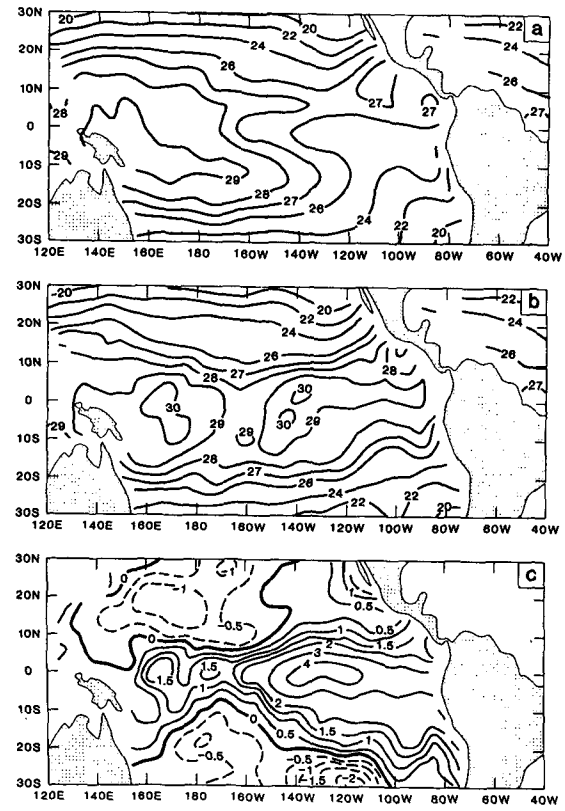

FIG. 6. January sea surface temperature (°C) for (a) climatology used in control integrations; (b) 1983 used in boundary integrations; and (c) observed anomaly for January, 1983. Dashed contours are negative.

present in the IC. However, this method automatically removes the model climate drift, assuming it is identical in the control and the boundary simulations. All boundary minus control (hereafter, B − C) fields shown in this section are time averages for the first 60 days of the integrations.

The second type of simulated anomaly, to be referred to as the forecast anomaly, is calculated by subtracting the 60-day mean observed climatology and the zonally averaged model climate drift from the 60-day mean model forecasts. For brevity the three types of anomalies examined here can be defined as follows,

boundary forced anomaly: $B - C$

observed anomaly: $O - OC$

forecast anomaly: $B - (\overline{MC} - \overline{OC}) - OC$

where

- B average of three boundary simulations starting from 15, 16 and 17 December 1982, through 15 February 1983;
- C average of three control simulations starting from 15, 16 and 17 December 1982, through 15 February 1983;
- O observed NMC analysis from 15 December 1982, through 15 February 1983
- OC observed climatology: average of 5-yr of observed NMC analyses (1979, 1980, 1981, 1982, and 1984).
- MC model climatology: average of 5 model (control) simulations for 60 days each. The observed and the model climatologies are calculated for 60-day periods starting from 1 January of five different years (1979, 1980, 1981, 1982 and 1984).
- $\overline{OC}$ zonally averaged values of OC
- $\overline{MC}$ zonally averaged values of MC.

The forecast anomaly retains the contribution of the initial conditions in the 60-day mean forecast. We will show that the contribution of the initial conditions even for a 60-day mean forecast is not negligible. By comparing these results with earlier sensitivity studies using the same model, we will also show that use of the correct IC gives rise to a more realistic response due to the change in SST. It should be noted that the length of the model integrations used for calculation of the model drift is always identical to the length of the model forecasts, although they are not for the same calendar dates. This should not affect our results because the model drift is more a function of the length of integration time than the calendar date of the initial condition within a given season. To be consistent with the definition of the forecast anomaly and boundary minus control (B − C) anomaly, the observed anomalies shown in this section are calculated by subtracting the observed 60-day mean (16 December 1982 through 15 February 1983) NMC analysis from the 5-yr 60-day mean observed climatology discussed before. The observed precipitation anomalies shown here are an exception due to the lack of an analyzed precipitation dataset.

The observed December, January, February (DJF) 1982–83 precipitation anomalies shown in Fig. 7a are calculated from outgoing longwave radiation (OLR) anomalies based on a 7-yr OLR climatology. To facilitate comparison with model results, the empirical relation that a negative 5.7 W m^{-2} OLR anomaly corresponds to a positive 1 mm day^{-1} precipitation anomaly was used to obtain the anomalies in precipitation units (Arkin, personal communication). This empirical relation should be used with caution as it is based on just 7 yr of data over a small region in the tropical Pacific. All observed and simulated fields in the remainder of this section are time averages over the first 60 days of the simulations as previously discussed. The structure and the pattern of the model simulated precipitation anomaly (B − C, Fig. 7b) is remarkably similar to the observed precipitation anomaly. The large positive precipitation anomaly observed over the central and eastern tropical Pacific which was the most unusual feature of the tropical rainfall during the winter of 1982–83 is particularly well simulated. The negative anomaly over Indonesia–Australia and the negative–positive anomaly dipole over Brazil are also well simulated. The positive anomaly observed in the vicinity of 20°S, 120°W associated with an eastward shift in the SPCZ is not well simulated. This is not surprising in light of the poor simulation of the SPCZ in the model climatology (Fig. 4b). It should be noted that the B − C

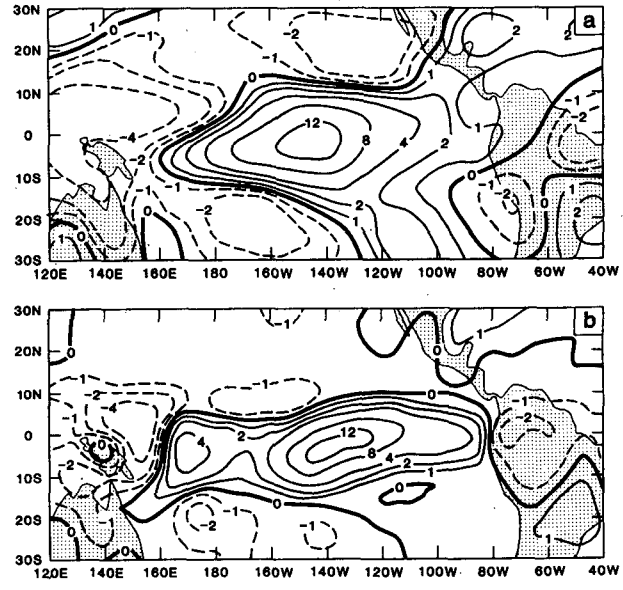

FIG. 7. (a) The DJF 1982–83 observed precipitation anomaly (mm day^{-1}) calculated from observed OLR anomaly. (b) 1–60 day average B − C precipitation difference. Contours are ±1, 2, 4, 8 and 12 mm day^{-1}. Dashed contours are negative.

precipitation differences were mainly due to the differences in the moisture flux convergence in the lower layers. However, positive latent heat flux differences of over 100 w m^{-2} occurred in the region 115°–150°W, 5°N–5°S.

In association with the precipitation anomalies strong (~10 m s^{-1}) low-level westerly wind anomalies were observed during the 1982–83 winter season in the central equatorial Pacific (Fig. 8a). The B − C wind field at 850 mb (Fig. 8b) correctly simulates these anomalies, as does the forecast anomaly wind field at 850 mb (Fig. 8c). However, a weak anomalous anticyclonic feature observed to the northwest, and a weak anomalous cyclonic feature to the southeast are simulated only in the forecast anomaly field.

The observed sea level pressure (SLP) anomaly field (Fig. 9a) contains a strong negative Southern Oscillation (SO) signal in the tropics, as well as large negative anomalies near the Aleutians, New Zealand, Iceland, northwestern Eurasia and the southern tip of Africa. The B − C SLP field (Fig. 9b) contains the strong SO signal in the tropics, but has weaker-than-observed

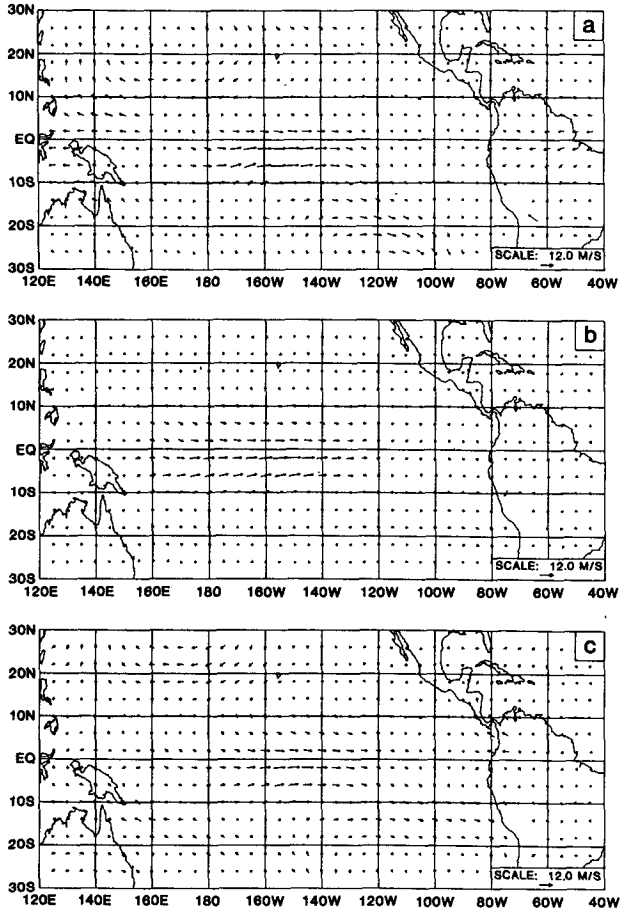

FIG. 8. 1–60 day average 850 mb wind (m s^{-1}) vectors for (a) observed anomaly; (b) B − C; and (c) forecast anomaly. Arrow at bottom represents 12 m s^{-1}.

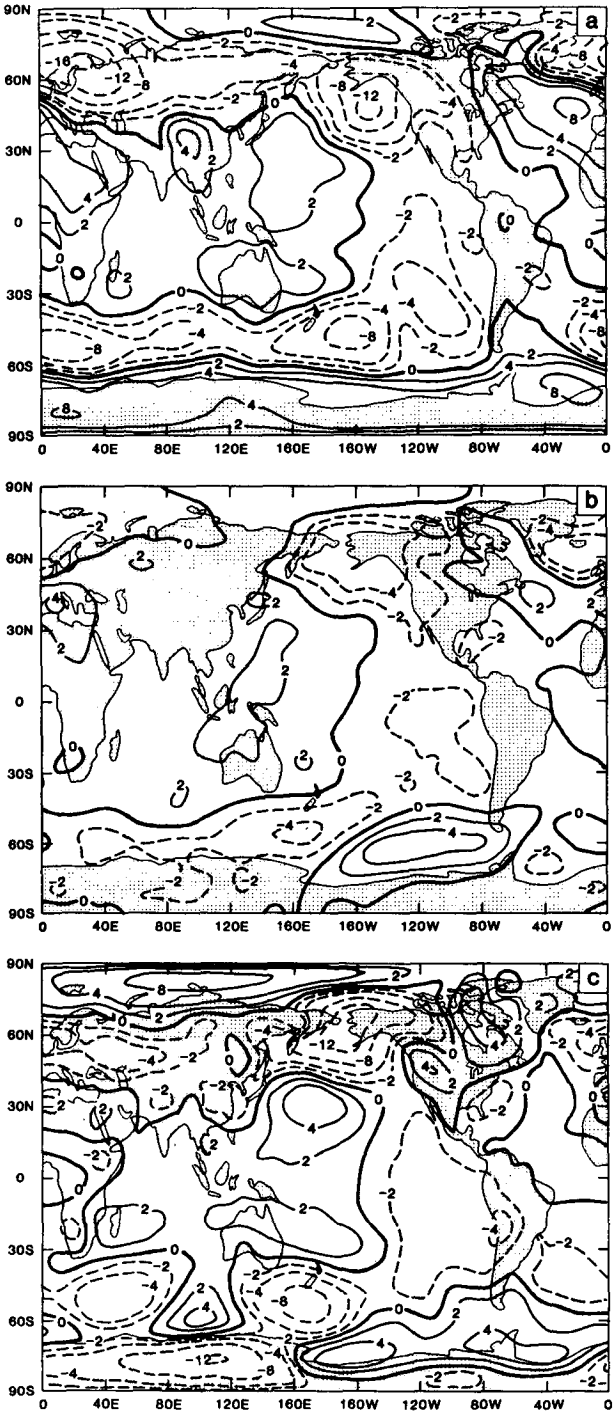

FIG. 9. 1–60 day average sea level pressure (mb) (a) observed anomaly; (b) B − C; and (c) forecast anomaly. Dashed contours are negative.

negative anomalies near the Aleutians, New Zealand and Iceland. The forecast anomaly SLP field (Fig. 9c) contains the strong SO signal as well as the other four observed strong extratropical negative anomalies; however, the forecast anomaly is not better than B − C

everywhere, as is the case over the southwestern United States. This occurs in regions where the model has similar local forecast errors in both B and C runs; thus, by taking the difference, B − C, this error is reduced.

The observed zonally averaged temperature anomaly cross section (Fig. 10a) contains a greater than 1 deg anomaly from the surface up to almost 200 mb in the tropics. This anomaly is likely due to the tropical heating anomaly associated with the precipitation anomaly. The B − C (Fig. 10b) and forecast anomaly (Fig. 10c) zonal temperature cross sections contain tropical anomalies of similar magnitude and extent, although they both place more of the anomaly in the upper atmosphere than observed. Negative anomalies in the observed zonal temperature cross section near 45°S and 80°N are only weakly represented in the simulated anomaly fields; however, observed positive anomalies poleward of 60°S are simulated reasonably well, particularly in the forecast anomaly field.

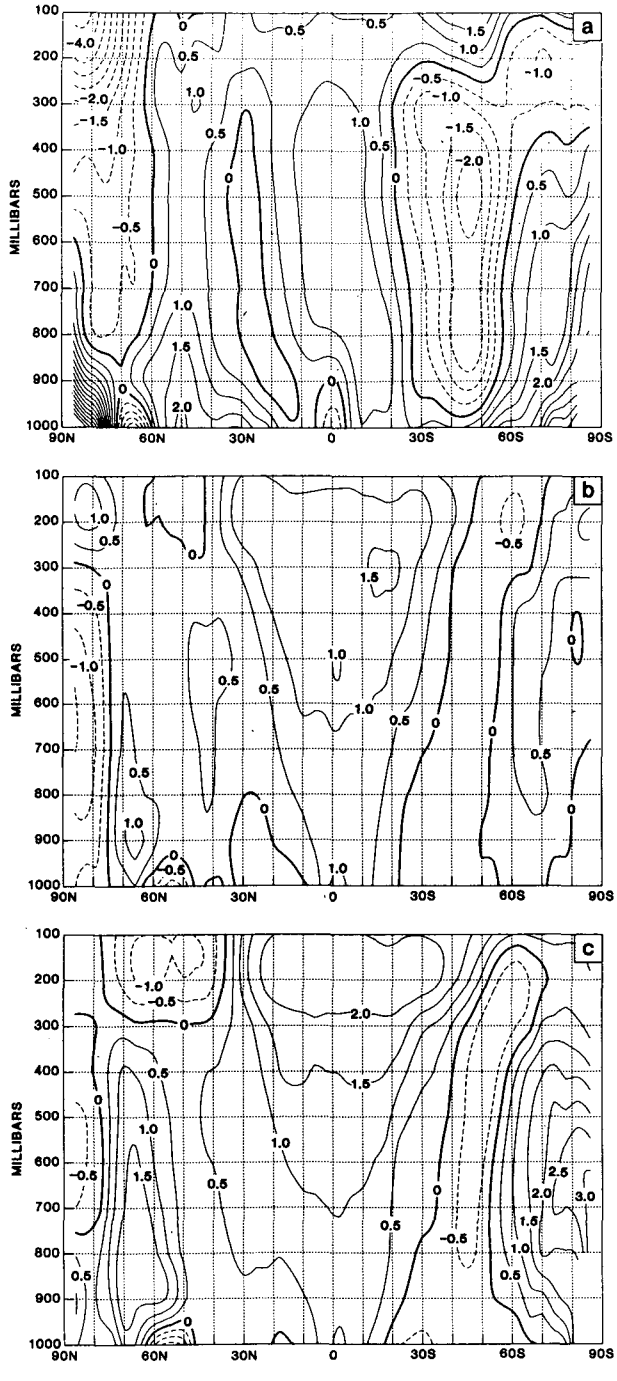

FIG. 10. 1–60 day average zonally averaged temperature (°C) for (a) observed anomaly; (b) B − C; and (c) forecast anomaly. Dashed contours are negative.

Both subtropical jets were anomalously strong in 1982–83 as evidenced by the observed, zonally averaged, zonal wind anomaly cross section (Fig. 11a). The B − C zonal wind cross section (Fig. 11b) also contains positive anomalies in the vicinity of the subtropical jets, but they are roughly half the magnitude of those observed. In the extratropics, the correspondence between the observed and the B − C fields is rather poor, although they both display a tendency for banding of positive and negative anomalies. The forecast anomaly zonal wind cross section (Fig. 11c) contains a remarkably good representation of the observed strengthening of the subtropical jets as well as the large decrease in the Southern Hemisphere midlatitude zonal winds.

The general pattern of increased subtropical jets and decreased zonal winds in midlatitudes can also be seen in the observed global 300-mb zonal wind anomaly field (Fig. 12a). Also evident in this field is the strong negative anomaly over the equatorial Pacific. This anomaly is not so prominent in the zonal average (Fig. 12a) because of cancellation with the positive anomalies over the equatorial Atlantic and Africa. The equatorial Pacific negative anomaly, the increased speeds of subtropical jets, the negative midlatitude anomalies and the positive anomalies in the tropics downstream are all represented in the B − C 300-mb zonal wind field (Fig. 12b) as well as in the forecast anomaly zonal wind field (Fig. 12c). There is a general tendency for these features to shift equatorward downstream, which partially explains why they are not all strongly represented in the zonally averaged fields. The reason the B − C field is better than the forecast anomaly field over Spain is because both the control and boundary simulations had large but similar errors which were reduced by taking the difference B − C.

The observed 300-mb height field contains large anomalies in both the tropics and the extratropics (Fig. 13a). An anomalous anticyclonic couplet straddles the equator in the Pacific and strong negative anomalies are flanking in middle latitudes. Over North America, a PNA type pattern (Wallace and Gutzler, 1981) is also evident. The B − C 300-mb geopotential height field (Fig. 13b) also contains these features. A similar B − C geopotential height anomaly field shown by Fennessy et al. (1985) failed to show any evidence of a PNA type pattern, even though they used the same model and

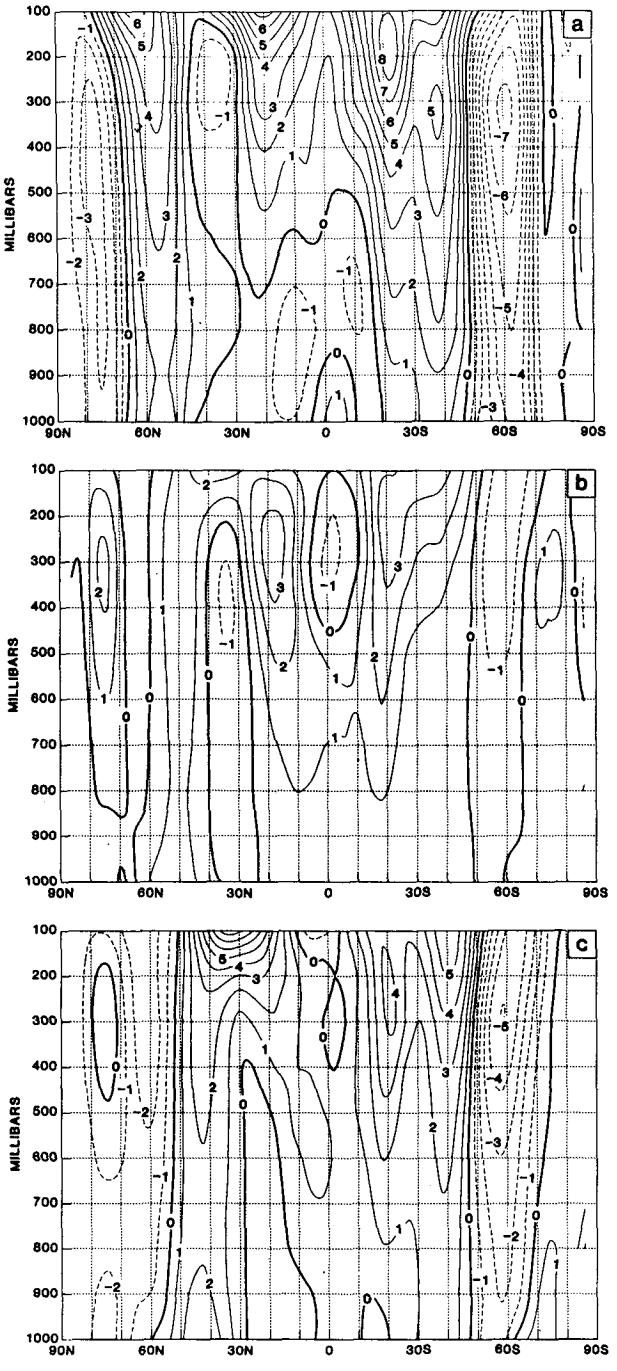

FIG. 11. 1–60 day average zonally averaged zonal wind (m s^{-1}) for (a) observed anomaly; (b) B − C; and (c) forecast anomaly. Dashed contours are negative.

the same boundary conditions. The only difference is that those simulations were performed with different initial conditions, whereas the current simulations are all initialized from the actual 1982 observations. By defining the anomaly as the difference between the boundary and the control simulations (B − C), the persistence effect of the initial conditions is automatically removed; however, the B − C 300 mb height field still shows a PNA type pattern as was observed. This suggests that in addition to the persistence effect, the observed initial conditions also produce a more

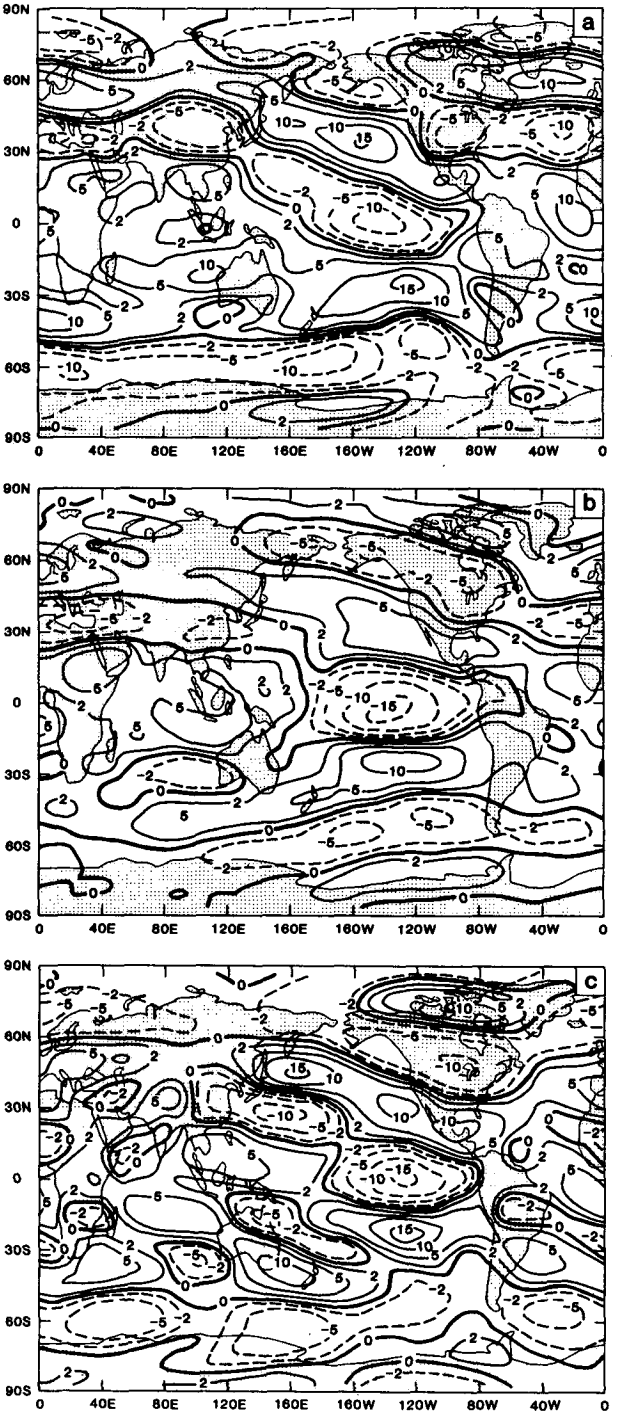

FIG. 12. 1–60 day average 300-mb zonal wind (m s^{-1}) for (a) observed anomaly; (b) B − C; and (c) forecast anomaly. Contours are ±2, 5, 10, and 15 m s^{-1}. Dashed contours are negative.

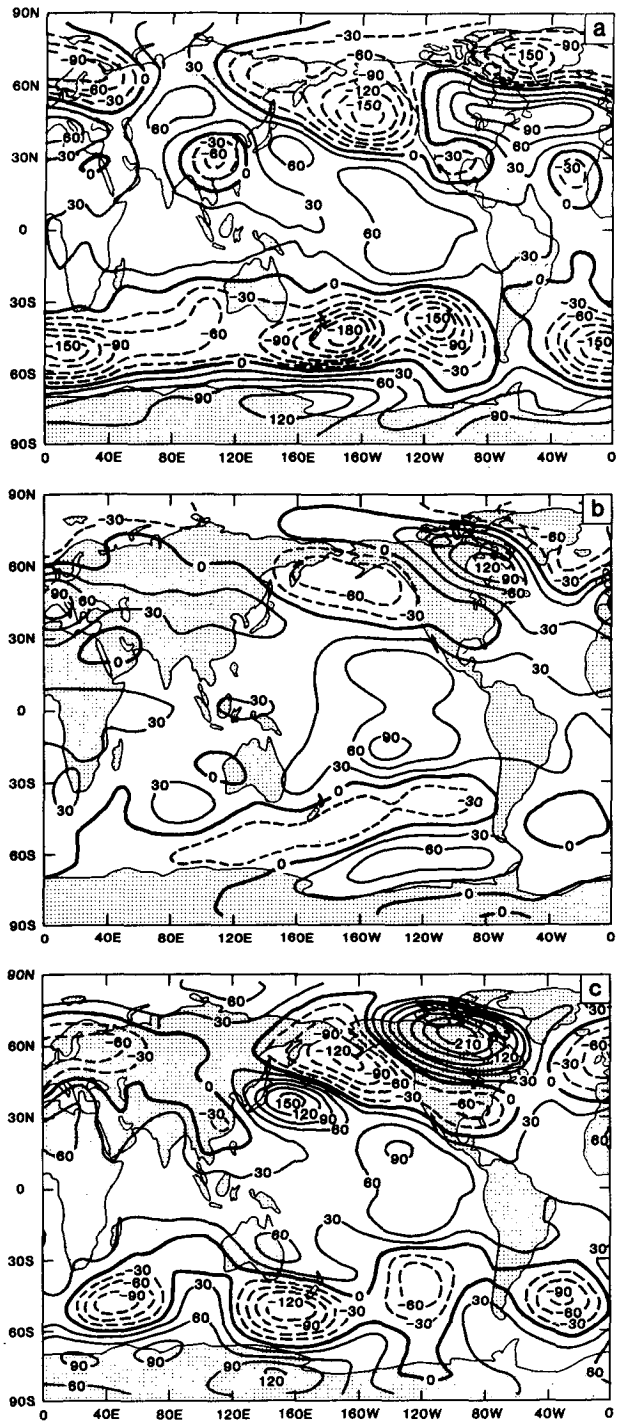

FIG. 13. 1–60 day average 300-mb geopotential height (meters) for (a) observed anomaly; (b) B − C; and (c) forecast anomaly. Dashed contours are negative.

correct evolution of the boundary forced circulation anomaly. As seen in Fig. 5b there were strong anomalies present in the initial conditions themselves; most notably, a very strong negative anomaly occurred in the vicinity of the Aleutian low, which had great persistence in the observations as well as in both the control and boundary simulations. Thus, even though the effect of the boundary conditions was to deepen this low, as seen in Fig. 13b, the resulting anomaly is small compared to that observed. The forecast anomaly 300-mb geopotential height field (Fig. 13c) contains a more realistic representation of the negative anomaly over the Aleutians as well as the negative anomaly near Texas and over western Asia. The positive anomaly over North America is not well positioned and is too strong compared to that observed. A band of negative anomalies in the Southern Hemisphere, and particularly the large negative anomaly near New Zealand are simulated reasonably well. We conjecture that a three-dimensional climate drift correction based on a much larger number of control integrations and observations could further improve the forecasts.

b. Time evolution of the circulation anomalies

The time evolution of the Northern Hemisphere midlatitude 300-mb geopotential height anomalies is presented in a longitude–time cross section constructed from nonoverlapping 5-day means. In Fig. 14, longitude–time cross sections of 300-mb geopotential height averaged from 44°N to 56°N are presented for (a) observed anomaly; (b) B − C; and (c) forecast anomaly. These anomaly fields are calculated the same way as those discussed in the time-mean section of this paper, except that 5-day means are used for all components of this calculation instead of the 60-day means. The strong negative anomaly observed in the vicinity of the Aleutians (160°W, Figs. 13a, 14a) persisted throughout the 60-day period with the exception of a brief period around days 11–15. Both the B − C anomaly field as well as the forecast anomaly field also maintain this anomaly, although the forecast anomaly field (Fig. 14c) more closely resembles the one observed (Fig. 14a) than does the B − C field (Fig. 14b). The positive anomaly observed in the Hudson Bay area (80°–100°W, Figs. 13a, 14a) persisted through most of the 60-day period, although it shifted eastward during the last 15 days. The forecast anomaly field (Fig. 14c) correctly simulates the evolution of this feature whereas the B − C field (Fig. 14b) does not. Neither of the simulated anomaly fields closely resemble the observed field west of 160°E, although the forecast anomaly field is generally closer to the observations than the B − C field. Overall, the time evolution of the forecast anomaly appears to be a fair representation of the time evolution of the observed anomaly. The overall low magnitude of the B − C and forecast anomalies is mainly due to the averaging of the three cases, which were somewhat dissimilar.

To demonstrate the time evolution of selected features of the observed and simulated circulation, areally averaged 5-day running mean/time series are also presented. In Fig. 15, the observed time series is starred,

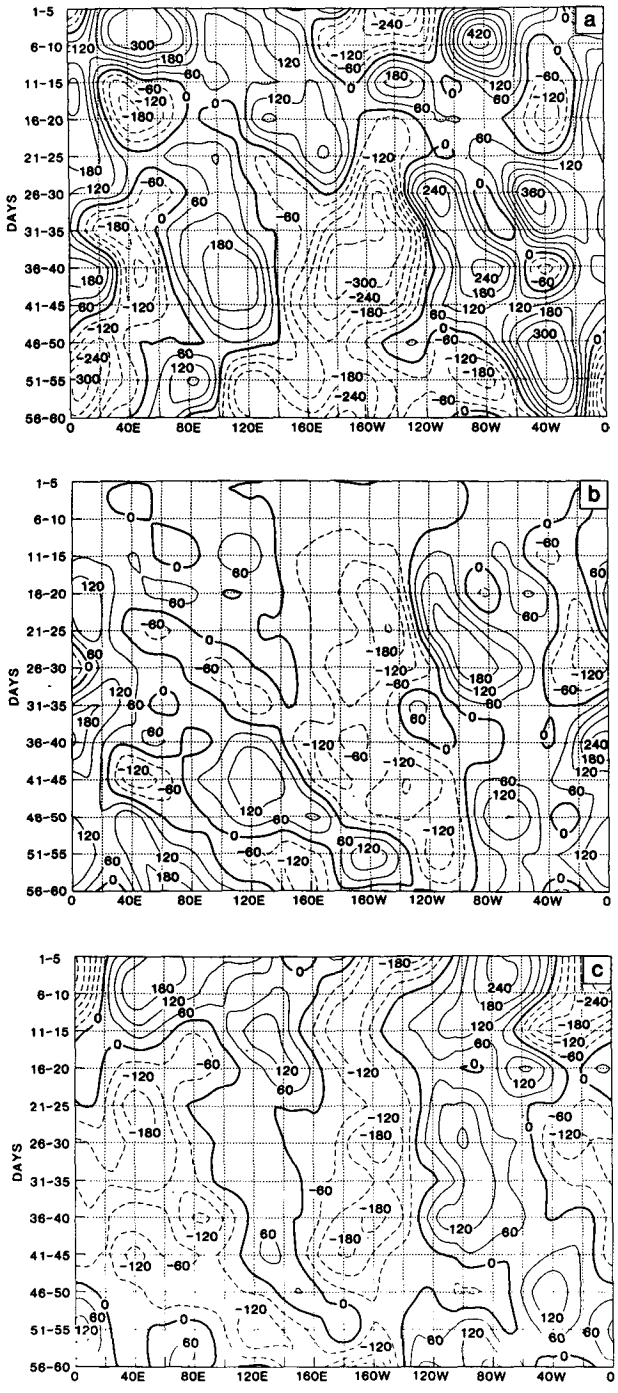

FIG. 14. Longitude–time cross section of 5-day averaged 44°–56°N 300-mb geopotential height (meters) for (a) observed anomaly; (b) B − C; and (c) forecast anomaly. Dashed contours are negative.

the individual control integrations are light dashed, the average of the three control integrations is heavy dashed, the individual boundary integrations are light solid and the average of the three boundary integrations is heavy solid.

In 1982–83 a precipitation anomaly dipole with anomalously strong precipitation in the eastern Pacific and anomalously weak precipitation in the western Pacific was observed. The curves in Fig. 15a depict the time evolution of this dipole [eastern Pacific (8°N–8°S, 127.5°–157.5°W) minus western Pacific (8°N–8°S, 127.5°–157.5°E) precipitation anomaly]. The observed precipitation used for Fig. 15a was calculated from the OLR time series using the empirical formula described earlier. Before taking the difference, the areally averaged precipitation used for all nine curves displayed in Fig. 15a was put in anomaly form by subtracting the appropriate monthly mean observed climatological precipitation. This observed climatological precipitation was obtained using the same 7-yr OLR climatology and the same empirical formula used for Fig. 4a. The curves for the control integrations hover around zero, indicating near climatological values for this index. The boundary integrations immediately begin to develop the observed anomaly dipole, and from day 25 onward contain an anomaly dipole which is very similar to that observed. It is noteworthy that the three integrations with different initial conditions are quite close to each other for the control as well as for the boundary integrations, suggesting that the tropical rainfall is strongly influenced by the boundary conditions.

A record negative Southern Oscillation index was observed during the winter of 1982–83 (Quiroz, 1983). A measure of the tropical Pacific SLP anomaly dipole is shown in Fig. 15b in which the curves display the difference (eastern Pacific (8°N–8°S, 117.5°–97.5°W) minus western Pacific (8°N–8°S, 122.5°–142.5°E) SLP anomaly. Before taking this difference, the areally averaged data used for all nine curves was put in anomaly form by subtracting the observed January climatological SLP (Godbole and Shukla, 1981). For the control integrations, this index is initially near zero, but has a slight negative trend due to a negative drift in the model climatological eastern Pacific SLP. It immediately becomes negative in the boundary integrations and is very close to the observed index throughout the 60-day period. It should be noted again that the effect of changing the boundary condition is much larger than that of changing the initial conditions in the tropics.

The development of the tropical temperature anomaly can be inferred from the time series of 200–1000 mb thickness averaged zonally and from 30°S to 30°N (Fig. 15c). Although the tropical atmosphere in the boundary integrations is still cold relative to that observed, it immediately warms up relative to that in the control integrations. Overall, the tropical temperature error has been roughly halved by the inclusion of the observed SST in the boundary integrations.

The central equatorial Pacific (8°N–8°S, 157.5°–137.5°W) 200-mb zonal wind is shown in Fig. 15d. The observed time series shows negative (easterly) zonal winds for the entire period. The zonal wind in this

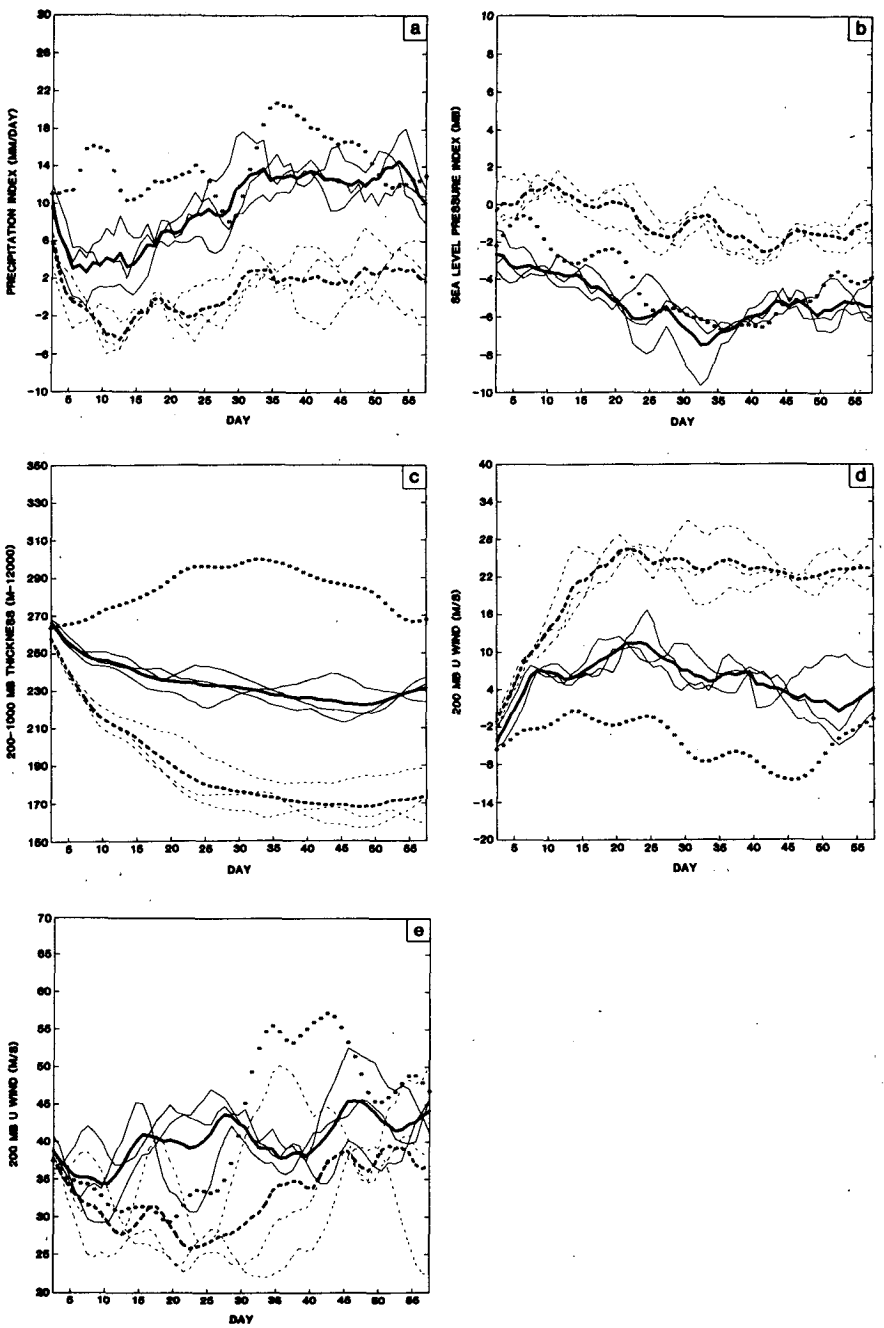

FIG. 15. A 5-day running mean time series of (a) E–W Pacific precipitation (mm day^{-1}) anomaly index; (b) E–W Pacific sea level pressure (mb) index; (c) Zonally averaged 30°N–30°S 200–1000 mb thickness (meters); (d) central equatorial Pacific 200 mb zonal wind (m s^{-1}); and (e) Northern Hemisphere subtropical jet region, 200-mb, zonal wind (m s^{-1}). Control integrations are dashed (average of three, heavy dashed). Boundary integrations are solid (average of three, heavy solid). Observations are starred.

region remains westerly in the boundary integrations; however, its magnitude is greatly reduced relative to that in the control integrations. The zonal wind in the control integrations is westerly and far too large in magnitude.

The 200-mb zonal wind in the vicinity of the Northern Hemisphere subtropical jet (24°–40°N, 157.5°–137.5°W) is shown in Fig. 15e. Unlike the previously shown tropical time series, the individual initial conditions for control and boundary integrations are not

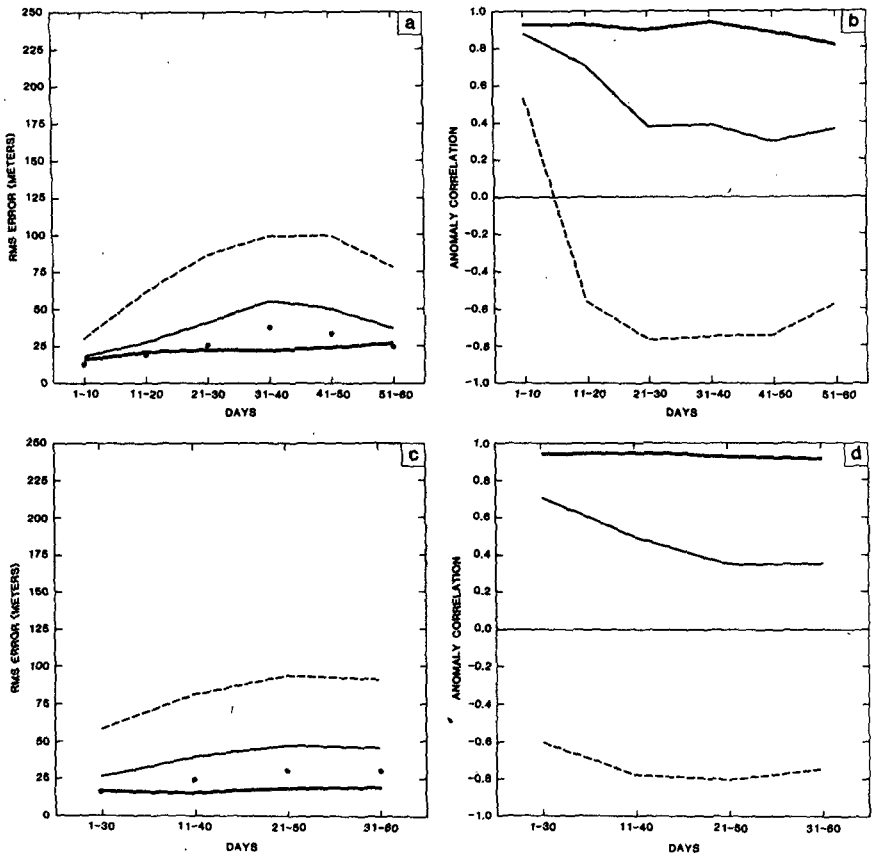

FIG. 16. The rms error (meters) and anomaly correlation coefficients (ACC) for tropical region (20°S–20°N) for 300 mb. (a) rms error for 10-day mean; (b) ACC for 10-day mean; (c) rms error for 30-day mean; and (d) ACC for 30-day mean. Average of control integrations is dashed; average of boundary integrations is solid; average of boundary integrations minus zonally averaged climate drift is heavy solid, and persistence is starred.

clustered close to their means; this is indicative of the much higher variability in midlatitudes due to small changes in the initial conditions. However, the zonal wind for the boundary integrations is closer to the observations for days 1–10 and 25–60. During days 10–25, the control simulations are closer to the observations compared to the boundary simulations. During days 30–45, the zonal wind for even the boundary simulations remains low compared to the extremely strong observed winds. The most remarkable feature of this figure is the large variability due to different initial conditions.

c. *The root-mean-square error and anomaly correlation coefficients*

The first 60 days of the average control and average boundary integrations are compared to the observations for the same period, 16 December 1982–15 February 1983. The rms error and ACC for the average of three integrations for 300-mb geopotential height are presented for the following five types of forecasts:

1) control integrations with climatological boundary conditions and no removal of the zonal mean climate drift (CONT);

2) boundary integrations with the observed SST anomaly in the Pacific Ocean and no removal of the zonal mean climate drift (BOUND);

3) control integrations with climatological boundary conditions and removal of the zonal mean climate drift (C − ZD);

4) boundary integrations with the observed SST anomaly in the Pacific Ocean and removal of the zonal mean climate drift (B − ZD);

5) persistence (PERS).

The observed climatology previously described is used as the basis for all ACC calculations. The results for nonoverlapping 10- and 30-day means are shown in Figs. 16, 17, 18 and 19. The results for the 60-day mean forecasts are given in Table 1. In Table 1, the results are given from left to right for CONT, BOUND, C − ZD, B − ZD, and PERS. The ACC is not presented

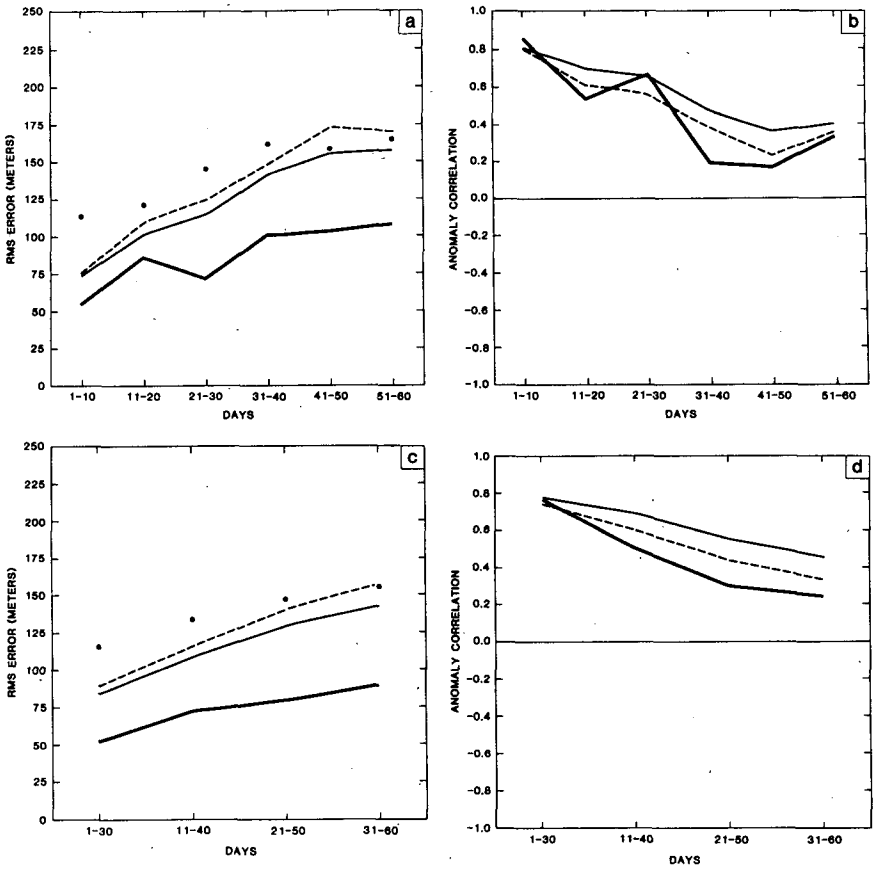

FIG. 17. The rms error (meters) and anomaly correlation coefficients (ACC) for Southern Hemisphere midlatitude region (20°–76°S) for 300 mb. (a) The rms error for 10-day mean; (b) ACC for 10-day mean; (c) The rms error for 30-day mean; and (d) ACC for 30-day mean. Average of control integrations is dashed; average of boundary integrations is solid; average of boundary integrations minus zonally averaged climate drift is heavy solid, and persistence is starred.

for the persistence forecast. These calculations are reported for four regions, which, going down a column in Table 1 are tropics (20°S–20°N), Southern Hemisphere (20°–76°S), Northern Hemisphere (20°–76°N) and Pacific–America sector (58°S–58°N, 60°–180°W). The 10- and 30-day mean values for the same four regions are presented in Figs. 16, 17, 18 and 19, respectively. In these figures, persistence (rms only) is starred, C is dashed, B is light solid and B − ZD is heavy solid. In Figs. 16–19, C − ZD is not shown in order to make the figures more readable. As shown in Table 1, the improvements in the control forecast made by removing the zonally averaged model climate drift are comparable to that made by removing the zonally averaged model climate drift from boundary forecasts (B).

In the tropics (Table 1 and Fig. 16), the effect of the SST anomaly is to greatly improve the forecast (rms and ACC) for all time means. Because of a strong negative climate drift in the tropics, the ACC becomes negative for the control integrations. However, only after removing the zonally averaged model climate drift does the tropical forecast become better than persistence for rms.

In the Southern Hemisphere (Table 1 and Fig. 17), the effect of the SST anomaly is to slightly improve the forecast (rms and ACC) for all the time means. Removing the zonally averaged model climate drift in the Southern Hemisphere greatly reduces the rms errors, but also reduces the ACC. This seemingly contradictory result arises because the model climate drift in the Southern Hemisphere midlatitudes (Fig. 3) is very similar to the observed anomaly (Fig. 13a).

In the Northern Hemisphere (Table 1 and Fig. 18), the effect of including the SST anomaly is to improve the forecast (rms and ACC) for all the time means. Removing the model climate drift produces further improvement.

The Pacific–American sector (Table 1 and Fig. 19) was chosen because we expected the effects of the Pacific SST anomalies to be most prominent over that region. Thus, it is encouraging that our greatest forecast

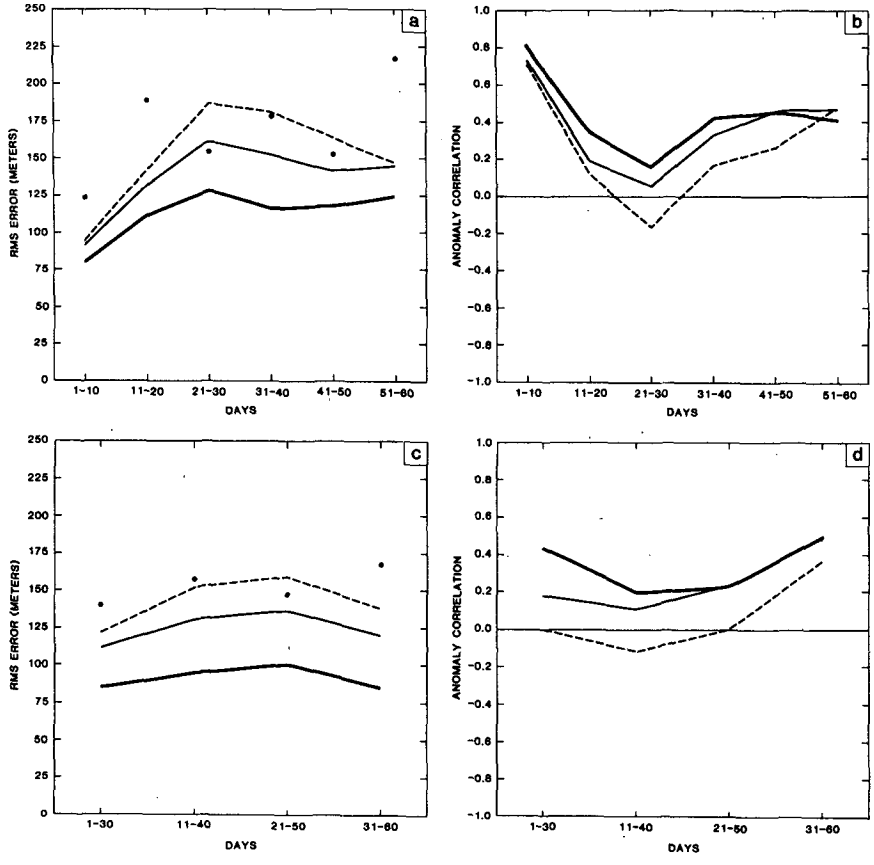

FIG. 18. The rms error (meters) and anomaly correlation coefficients (ACC) for Northern Hemisphere midlatitude region (20°–76°N) for 300 mb. (a) The rms error for 10-day mean; (b) ACC for 10-day mean; (c) The rms error for 30-day mean; and (d) ACC for 30-day mean. Average of control integrations is dashed; average of boundary integrations is solid; average of boundary integrations minus zonally averaged climate drift is heavy solid, and persistence is starred.

improvement by including the SST anomaly is obtained for this region.

6. Summary and concluding remarks

A global general circulation model was integrated for 60 days starting from five observed initial conditions at 0000 UTC on 1 January 1979, 1980, 1981, 1982 and 1984, with climatological, seasonally varying boundary conditions of SST, soil moisture, sea ice and snow cover. The differences between the model predictions and the actual observations for these five integrations were averaged to define the systematic error (climate drift) of the model. This climate drift contained much zonal asymmetric structure, although the asymmetric component of the forecast error was highly variable among the five cases. The zonally averaged forecast error was quite similar in all five cases, and therefore, the zonally averaged forecast error for all five cases was averaged to define a mean zonally averaged model climate drift, which could be later used to correct the model forecast produced from independent initial conditions.

The same model was used to examine the influence of Pacific Ocean SST anomalies on 10-, 30- and 60-day mean forecasts starting from the initial conditions at 0000 UTC on 15, 16 and 17 December 1982. For each of these three initial conditions, the model was first integrated for 60 days with climatological boundary conditions. The integrations were repeated after adding the observed SST anomalies over the Pacific Ocean during 1982–83. We have referred to these two sets of integrations as the control simulation and the boundary simulation, respectively.

We have examined the results from two different points of view:

(a) What is the effect of changing the SST boundary condition on atmospheric circulation and rainfall? To address this question we have examined the differences between the boundary and control simulations.

(b) What is the impact of the observed SST anomalies on actual prediction? To address this question we

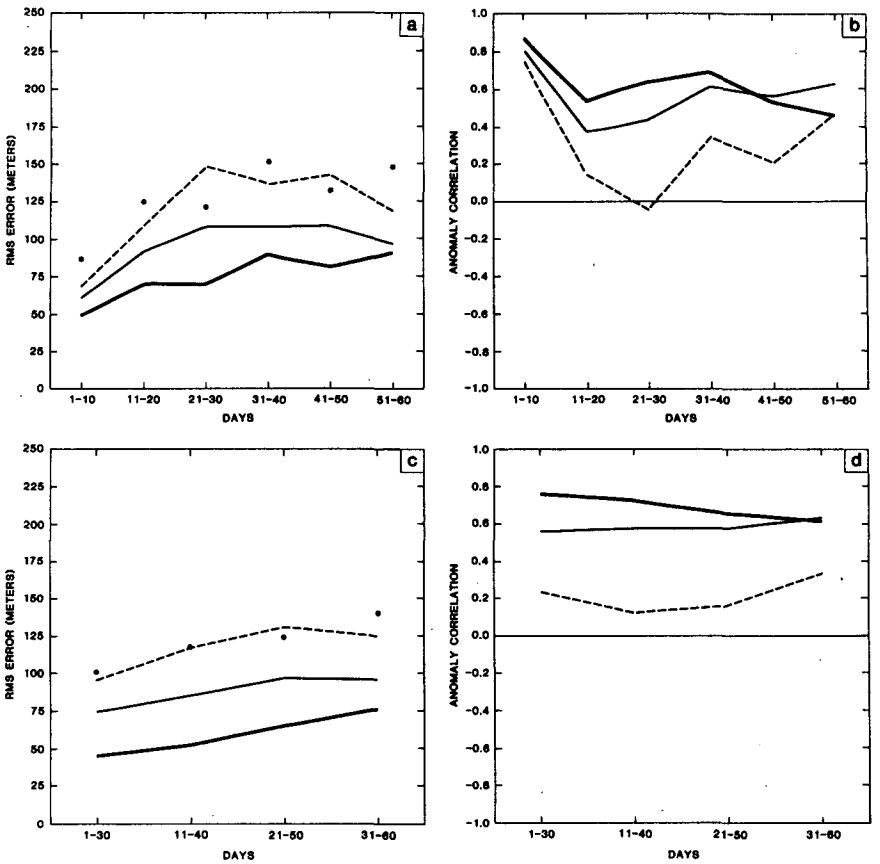

FIG. 19. The rms error (meters) and anomaly correlation coefficients (ACC) for Pacific–America region (58°S–58°N, 60°–180°W) for 300 mb. (a) The rms error for 10-day mean; (b) ACC for 10-day mean; (c) The rms error for 30-day mean; and (d) ACC for 30-day mean. Average of control integrations is dashed; average of boundary integrations is solid; average of boundary integrations minus zonally averaged climate drift is heavy solid, and persistence is starred.

compare the model forecasts with the corresponding observations. However, since the model has a large climate drift, we first remove a zonally symmetric climate drift from the model forecast before we compare the forecast anomalies with the observed anomalies.

It should be noted that (a) represents the classical sensitivity experiment in which the effects of the initial conditions are not considered to be of any particular importance, especially because the sensitivity experiments are carried out by integrating the model for a long period of time. The differences between the boundary and control integrations are not generally considered to be suitable for comparison with the observations because the dynamical structure of the large-scale flow from the initial conditions has been subtracted out. For 30–60 day mean forecasts, the initial conditions remain quite important in determining the monthly mean as well as in determining the nature of the response to a given boundary forcing. Therefore, in order to examine the impact of changes in the boundary conditions on predictions of time averaged circulation, it is more appropriate to examine (a) as well as (b), which contains the combined effects of the initial conditions and the boundary conditions.

We have examined the boundary forced anomaly and the forecast anomaly, and compared both with the corresponding observations. Based on these comparisons we can draw the following conclusions:

(i) Use of the observed SST anomalies over the Pacific Ocean produces a spectacular improvement in the prediction of tropical circulation and rainfall for 30 and 60 day averages. The improvement in prediction was clearly seen even in the first 10 days.

(ii) The tropical response of the SST anomaly does not change by changing the initial conditions; it is strongly forced by the boundary conditions.

(iii) Use of the observed SST anomalies also produces a clear but small improvement in the prediction of 30- and 60-day average circulation over the midlatitudes. The prediction is further enhanced by removing the zonally symmetric climate drift of the model. It is our conjecture that the forecasts could be further im-

TABLE 1. The root mean square (rms) error (meters) and anomaly correlation coefficient (ACC) for control integrations (CONT), boundary anomaly integrations (BOUND), control minus zonal drift (C − ZD), boundary minus zonal drift (B − ZD) and persistence (PERS).

Region	CONT	BOUND	C − ZD	B − ZD	PERS
			a. rms		
Tropics					
20°S–20°N, all long	75	35	41	16	22
Southern Hemisphere					
20°–76°S, all long	119	109	71	64	129
Northern Hemisphere					
20°–76°N, all long	121	106	81	70	145
Pacific America					
58°S–58°N, 60°–180°W	103	78	74	50	114
			b. ACC		
Tropics					
20°S–20°N, all long	−0.75	0.53	0.21	0.94	
Southern Hemisphere					
20°–76°S, all long	0.58	0.66	0.31	0.48	
Northern Hemisphere					
20°–76°N, all long	0.08	0.31	0.01	0.39	
Pacific America					
58°S–58°N, 60°–180°W	0.27	0.65	0.07	0.70	

proved by removing a three-dimensional climate drift which can be defined only from a large number of independent forecasts.

(iv) Unlike the tropical response, the structure of the initial conditions plays an important role in determining the nature of the midlatitude response.

Similarities between anomalies present in the initial conditions (e.g., Fig. 5b) and the forecast anomalies for days 1–30 and 31–60 (not shown) have led us to speculate that at least for this particular case, the effects of the initial conditions could be important even for days 31–60.

This speculation is further supported by Table 2, in which we have shown the average rms and ACC for the five control cases which comprise the previously described model climatology. After the first 10 or 20 days, the ACC in these control simulations is essentially zero, while for the forecast cases, the ACC remains positive for the most part in all three extratropical regions depicted in Figs. 17–19. While we cannot claim

TABLE 2. The root-mean-square (rms) error (meters) and anomaly correlation coefficient (ACC) for five control cases used in model climatology.

	Days									
Region	1–10	11–20	21–30	31–40	41–50	51–60	1–30	11–40	21–50	31–60
					a. rms					
Tropics										
20°S–20°N, all long	27	47	53	53	55	54	39	48	51	51
Southern Hemisphere										
20°–76°S, all long	87	138	159	185	196	201	113	145	166	180
Northern Hemisphere										
20°–76°N, all long	96	165	195	207	181	192	122	156	157	156
Pacific America										
58°S–58°N, 60°–180°W	72	118	143	153	153	153	93	119	128	131
					b. ACC					
Tropics										
20°S–20°N, all long	0.21	0.10	−0.04	0.01	−0.02	−0.01	0.05	−0.03	−0.02	0.02
Southern Hemisphere										
20°–76°S, all long	0.36	0.02	0.05	−0.01	0.04	0.01	0.05	0.02	0.07	0.02
Northern Hemisphere										
20°–76°N, all long	0.57	0.17	−0.05	−0.06	0.06	−0.05	0.16	−0.02	−0.02	−0.01
Pacific America										
58°S–58°N, 60°–180°W	0.48	0.11	0.02	−0.02	−0.03	−0.01	0.15	0.05	0.02	0.00

that this proves that the initial conditions definitely influence the 31–60 day forecast in all cases, it certainly seems to be so in this particular case.

(v) It is possible that the dynamical prediction of monthly and seasonal averages can be further enhanced by using global boundary conditions of SST, soil moisture, sea ice and snow cover.

(vi) Although the model used in this study displays a large climate drift, even a posteriori removal of the climate drift produces significant improvements in the forecasts. It is therefore likely that better models with less climate drift would further improve the 30–60 day mean forecasts.

Acknowledgments. The authors would like to thank Mr. Larry Marx for his help with the integrations and Dr. R. Reynolds of CAC for providing the SST anomalies used in this study. We are grateful to Ms. L. Rumburg for drafting the figures and to Ms. M. Schlichtig and Ms. M. Hopkins for their careful preparation of the manuscript. Finally, we would like to thank the reviewers for their constructive comments which we feel have helped improve this paper.

This research was supported by the NASA climate program (NAGW-557) and NSF Grant ATM-8414660.

REFERENCES

Arakawa, A., 1969: Parameterization of cumulus convection. *Proc. WMO/IUGG Symp. on Numerical Prediction,* Tokyo, 1–6.

Blackmon, M. L., J. E. Geisler and E. J. Pitcher, 1983: A general circulation model study of January climate anomaly patterns associated with interannual variation of equatorial Pacific sea surface temperatures. *J. Atmos. Sci.,* **40,** 1410–1425.

Boer, G. J., 1985: Modelling the Atmospheric Response to the 1982/83 El Niño. *Coupled Ocean-Atmosphere Models.* J. C. J. Nihoul, Ed., Elsevier, 7–17.

Charney, J. G., and J. Shukla, 1981: Predictability of monsoons. *Monsoon Dynamics,* Sir James Lighthill and R. P. Pearce, Eds., (Proc. of a symp. at New Delhi, India, Dec., 1977.), Cambridge University Press, pp. 99–110.

Cubash, U., 1985: The mean response of the ECMWF global model to the El-Niño anomaly in extended range prediction. *Atmos.-Ocean,* **23,** 43–66.

Deardorff, J. W., 1972: Parameterization of the planetary boundary layer for use in general circulation models. *Mon. Wea. Rev.,* **100,** 93–106.

Fennessy, M. J., L. Marx and J. Shukla, 1985: General circulation model sensitivity to 1982–83 equatorial pacific sea surface temperature anomalies. *Mon. Wea. Rev.,* **113,** 858–864.

Geisler, J. E., M. L. Blackmon, G. T. Bates and S. Munoz, 1985: Sensitivity of January climate response to the magnitude and position of equatorial Pacific sea surface temperature anomalies. *J. Atmos. Sci.,* **42,** 1037–1049.

Godbole, R. V., and J. Shukla, 1981: Global analysis of January and July sea level pressure. NASA Tech. Memo. 82097. [NTIS N8124674.]

Hoskins, B. J., and D. Karoly, 1981: The steady linear response of a spherical atmosphere to thermal and orographic forcing. *J. Atmos. Sci.,* **38,** 1179–1196.

Julian, P. R., and R. W. Chervin, 1978: A study of the Southern Oscillation and Walker circulation phenomenon. *Mon. Wea. Rev.,* **106,** 1433–1451.

Keshavamurty, R. N., 1982: Response of the atmosphere to sea surface temperature anomalies over the equatorial Pacific and the teleconnections of the Southern Oscillation. *J. Atmos. Sci.,* **39,** 1241–1254.

Michaud, R., T. N. Krishnamurti, and R. Sadourny, 1985: Preliminary experiments on the sensitivity of atmospheric monthly mean prediction to sea-surface temperature specification. *Coupled Ocean Atmosphere Models,* J. C. J. Nihoul, Ed., Elsevier, (Elsevier Oceanography Series, 40.) 591–611.

Miyakoda, K., J. Sirutis and J. Ploshay, 1986: Monthly Forecast Experiments: Part I. Without anomaly boundary forcings. *Mon. Wea. Rev.,* **114,** 2363–2401.

Namias, J., 1978: Multiple causes of the North American abnormal winter 1967–77. *Mon. Wea. Rev.,* **106,** 279–295.

Palmer, T. N., and D. A. Mansfield, 1984: Response of two atmospheric general circulation models to sea-surface temperature anomalies in the tropical East and West Pacific. *Nature,* **310,** 483–485.

——, and ——, 1986a: A study of wintertime circulation anomalies during past El-Niño events using a high resolution general circulation model. Part I: Influence of model climatology. *Quart. J. Roy. Meteor. Soc.,* **112,** 613–638.

——, and ——, 1986b: A study of wintertime circulation anomalies during past El-Niño events using a high resolution general circulation model. Part II: Variability of the seasonal mean response. *Quart. J. Roy. Meteor. Soc.,* **112,** 639–660.

Quiroz, R. S., 1983: The climate of the "El-Niño" winter of 1982–83, a season of extraordinary climatic anomalies. *Mon. Wea. Rev.,* **111,** 1685–1706.

Randall, D. A., 1976: The interaction of the planetary layer with large-scale circulations. Ph.D. thesis, UCLA, 247 pp.

Rowntree, P. R., 1972: The influence of tropical east Pacific Ocean temperatures on the atmosphere. *Quart. J. Roy. Meteor. Soc.,* **98,** 290–321.

——, 1979: The effects of changes in ocean temperature on the atmosphere. *Dyn. Atmos. Oceans,* **3,** 373–390.

Shukla, J. 1981: Dynamical predictability of monthly means. *J. Atmos. Sci.,* **38,** 2547–2572.

——, 1983: On physical basis and feasibility of monthly and seasonal prediction with a large GCM. *Proc. WMO-CAS/JSC Expert Study Conf. on Long Range Forecasting, LRF Publ. Ser. No. 1,* WMO, Geneva 5, Switzerland, 142–153.

——, 1984: Predictability of time averages: Part II. The influence of the boundary forcing. *Problems and Prospects in Long and Medium Range Weather Forecasting.* (Proc. of a workshop at Reading, U.K.), D. M. Burridge and E. Kallen, Eds., Springer Verlag, 155–206.

——, 1986: SST anomalies and blocking. *Anomalous Atmospheric Flows and Blocking., Advances in Geophysics,* **40,** 443–452.

——, and J. M. Wallace, 1983: Numerical simulation of the atmospheric response to equatorial Pacific sea surface temperature anomalies. *J. Atmos. Sci.,* **40,** 1613–1630.

Suarez, M. J., 1985: A GCM study of the atmospheric response to tropical SST anomalies. *Coupled Ocean-Atmosphere Models.* J. C. J. Nihoul, Ed., Elsevier, 749–764.

Tokioka, T., K. Yamazaki and M. Chiba, 1985: Atmospheric response to the sea surface temperature anomalies observed in early summer of 1983. *J. Meteor. Soc. Japan,* **63,** 565–588.

Wallace, J. M., and D. S. Gutzler, 1981: Teleconnections in the geopotential height field during the Northern Hemisphere winter. *Mon. Wea. Rev.,* **109,** 784–812.

Walsh, John E., W. H. Jasperson and B. Ross, 1985: Influences of snow cover and soil moisture on monthly air temperature. *Mon. Wea. Rev.,* **113,** 756–768.

Webster, P. J., 1981: Mechanisms determining the atmospheric response to sea surface temperature anomalies. *J. Atmos. Sci.,* **38,** 554–571.